Design and experimental validation of a simple controller for a multi-segment magnetic crawler robot

Leah Kelley[*a], Saam Ostovari[**b], Aaron B. Burmeister[b], Kurt A. Talke[b],
Narek Pezeshkian[b], Amin Rahimi[b], Abraham B. Hart[b], Hoa G. Nguyen[b]

[a]Massachusetts Institute of Technology, 77 Massachusetts Ave, Cambridge, MA USA 02139;
[b]Space and Naval Warfare (SPAWAR) Systems Center Pacific, San Diego, CA USA 92152

ABSTRACT

A novel, multi-segmented magnetic crawler robot has been designed for ship hull inspection. In its simplest version, passive linkages that provide two degrees of relative motion connect front and rear driving modules, so the robot can twist and turn. This permits its navigation over surface discontinuities while maintaining its adhesion to the hull. During operation, the magnetic crawler receives forward and turning velocity commands from either a tele-operator or high-level, autonomous control computer. A low-level, embedded microcomputer handles the commands to the driving motors.

This paper presents the development of a simple, low-level, leader-follower controller that permits the rear module to follow the front module. The kinematics and dynamics of the two-module magnetic crawler robot are described. The robot's geometry, kinematic constraints and the user-commanded velocities are used to calculate the desired instantaneous center of rotation and the corresponding central-linkage angle necessary for the back module to follow the front module when turning. The commands to the rear driving motors are determined by applying PID control on the error between the desired and measured linkage angle position. The controller is designed and tested using Matlab Simulink. It is then implemented and tested on an early two-module magnetic crawler prototype robot. Results of the simulations and experimental validation of the controller design are presented.

Keywords: magnetic, crawler, robot, ship hull inspection, tank inspection

1. INTRODUCTION

Routine inspection of ship surfaces, including the hull, deck and tanks, for corrosion, damage and micro-fractures is an integral part of ship maintenance. Such inspections are labor-intensive and expensive. A magnetic robot equipped with the proper sensors may accomplish this task more quickly and at a much lower cost.

Magnetic climbing robots for inspection of ferromagnetic surfaces have been designed and tested.[1-13] Such designs use either magnetic wheels or tracks,[1-5,7,10-12] mount magnets in a central plate within the robot that can be raised and lowered in order to vary the magnetic-adhesive force,[6,9,13] or use a combination of several mobile units to facilitate climbing.[8] The majority of these robots are restricted to operation on smooth surfaces that are either flat or have large radii of curvature. Many cannot manage wall-to-wall or wall-to-ceiling corner transitions. Of those that can, the magnetic snake-like robots constructed to date cannot follow curved paths since they have minimal to no lateral flexibility.[10,12,13] The Magnebike robot can negotiate corner transitions uses a lifting mechanism to detach its front wheel momentarily from the magnetic surface to facilitate the corner transitions.[1,2] However, these robots are unable to negotiate ribbed surfaces (see Figure 1). Groups of reconfigurable modular robots have been proposed for negotiating complex structures, but have yet to be demonstrated.[14]

The Unmanned Systems Group at SPAWAR Systems Center Pacific has developed a multi-segment magnetic crawler robot (MSMR) capable of traversing the complex metal surfaces found in both marine vessels and transport tanks without losing adhesion[16] (see Figure 2). In its simplest configuration, it consists of two driving modules connected by a roll-yaw-bow linkage, as shown in Figure 3. Each drive module has a pair of magnetic wheels that provides

_____

[*] lckelley@mit.edu
[**] saam.ostovari@navy.mil

Report Documentation Page		*Form Approved* *OMB No. 0704-0188*

1. REPORT DATE **APR 2015**	2. REPORT TYPE	3. DATES COVERED **00-00-2015 to 00-00-2015**

4. TITLE AND SUBTITLE **Design and Experimental Validation of a Simple Controller for a Multi-segment Magnetic Crawler Robot**	5a. CONTRACT NUMBER
	5b. GRANT NUMBER
	5c. PROGRAM ELEMENT NUMBER
6. AUTHOR(S)	5d. PROJECT NUMBER
	5e. TASK NUMBER
	5f. WORK UNIT NUMBER
7. PERFORMING ORGANIZATION NAME(S) AND ADDRESS(ES) **Space and Naval Warfare Systems Center Pacific,53560 Hull Street,San Diego,CA,92152**	8. PERFORMING ORGANIZATION REPORT NUMBER
9. SPONSORING/MONITORING AGENCY NAME(S) AND ADDRESS(ES)	10. SPONSOR/MONITOR'S ACRONYM(S)
	11. SPONSOR/MONITOR'S REPORT NUMBER(S)

12. DISTRIBUTION/AVAILABILITY STATEMENT
Approved for public release; distribution unlimited

13. SUPPLEMENTARY NOTES

14. ABSTRACT

A novel, multi-segmented magnetic crawler robot has been designed for ship hull inspection. In its simplest version passive linkages that provide two degrees of relative motion connect front and rear driving modules, so the robot can twist and turn. This permits its navigation over surface discontinuities while maintaining its adhesion to the hull. During operation, the magnetic crawler receives forward and turning velocity commands from either a tele-operator or high-level, autonomous control computer. A low-level, embedded microcomputer handles the commands to the driving motors. This paper presents the development of a simple, low-level, leader-follower controller that permits the rear module to follow the front module. The kinematics and dynamics of the two-module magnetic crawler robot are described. The robot???s geometry, kinematic constraints and the user-commanded velocities are used to calculate the desired instantaneous center of rotation and the corresponding central-linkage angle necessary for the back module to follow the front module when turning. The commands to the rear driving motors are determined by applying PID control on the error between the desired and measured linkage angle position. The controller is designed and tested using Matlab Simulink. It is then implemented and tested on an early two-module magnetic crawler prototype robot. Results of the simulations and experimental validation of the controller design are presented.

15. SUBJECT TERMS

16. SECURITY CLASSIFICATION OF:			17. LIMITATION OF ABSTRACT	18. NUMBER OF PAGES	19a. NAME OF RESPONSIBLE PERSON
a. REPORT **unclassified**	b. ABSTRACT **unclassified**	c. THIS PAGE **unclassified**	**Same as Report (SAR)**	**13**	

adhesion on ferrous surfaces. The wheels are driven independently of one another, making each module differentially driven. The roll-yaw-bow linkage provides surface adaptability by permitting relative twisting and turning between the modules without requiring additional motors. The drive modules contain batteries, control electronics, microcomputers, sensors and wireless communication.

Figure 1. Ribbed surfaces of the guided missile cruiser USS Vella Gulf (CG 72).[15]

Figure 2. MSMR prototype on shipping containers.

Figure 3. A two-module MSMR prototype on underside of stairwell. A pan-tilt-zoom camera and light system has also been installed.

Since each wheel is individually driven, it is difficult for a tele-operator to directly control each motor using a standard RC controller, as was found during initial prototype testing. Coordinated motion control between the front and successive drive modules is needed. Initially, a simple control algorithm that permits the rear module to follow the front module is desired. Leader-follower control has been applied to snake robots.[17] In such research, the system kinematic equations are used to calculate the position of each robot segment at the next time step. The individual segments are then commanded to these positions. Experimental results show that this method results in imperfect following, especially as more segments are added.[17] Other methods of controlling snake-like robots include Lyapunov methods, shape controllable points, and other kinematic methods.[18-21] Many of these approaches are complex and may not be needed for the MSMR.

The MSMR leader-follower configuration is similar to a tractor pulling a trailer. Kinematics, dynamics and trajectory following control for tractors pulling one to several trailers have been studied.[18, 22-29] However, the trailers are typically passive, so actuators are limited to the driving wheels and steering of the tractor vehicle. In some instances, the trailers are also steerable, but have no drive power. Although the solutions presented to the tractor-trailer problem are not directly applicable to the MSMR, a similar kinematic-based approach to the leader-follower control problem is applied here.

This paper describes the development of a simple leader-follower controller that permits the rear module to follow the front module. Here, the robot's geometry, kinematic constraints and the user-commanded velocities are used to calculate the desired instantaneous center of rotation the robot is to follow, and the corresponding central linkage angle necessary for the back module to follow the front module when turning. The commands to the rear driving motors are determined by applying proportional-integral-derivative (PID) control on the error between the desired and measured linkage angle position. The controller is tested in simulation and on an early MSMR prototype.

2. ROBOT KINEMATIC ANALYSIS

This section presents the MSMR kinematics. For this analysis, consider the robot motion on a planar magnetic surface, shown in Figure 4. In this case rotation about the roll axis is ignored and only rotation of the yaw axis is considered. Assume that the magnetic adhesion force is sufficient to keep the robot in contact with the metal surface, and that the
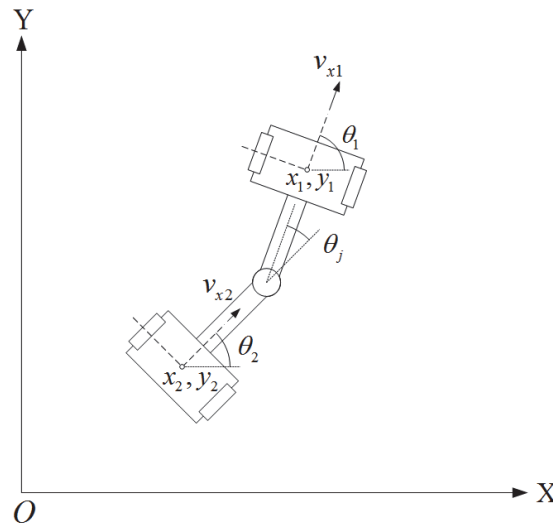

Figure 4. The MSMR position in an inertial frame.

robot doesn't slip.

The robot position in an inertial frame aligned with the magnetic surface is fully described by the vector $\mathbf{q}$:

$$\mathbf{q} = \begin{bmatrix} x_1 & y_1 & \theta_1 & \theta_2 \end{bmatrix}^T \tag{1}$$

where x_1 and y_1 are the coordinates of the front module center of mass, assumed located in the front drive module's geometric center, and θ_1 and θ_2 are the orientations of the front and rear modules, respectively. The position of the rear module, (x_2, y_2), is related to the position of the front module by

$$x_2 = x_1 + d_1 \cos\theta_1 + d_2 \cos\theta_2$$
$$y_2 = y_1 + d_1 \sin\theta_1 + d_2 \sin\theta_2$$

(2)

where d_1 and d_2 are the distances from the front and rear module centers of mass to the yaw joint, respectively. Differentiating equation (2) yields the linear velocities, $(\dot{x}_2, \dot{y}_2)$, of the second module:

$$\dot{x}_2 = \dot{x}_1 - \dot{\theta}_1 d_1 \sin\theta_1 - \dot{\theta}_2 d_2 \sin\theta_2$$
$$\dot{y}_2 = \dot{y}_1 + \dot{\theta}_1 d_1 \cos\theta_1 + \dot{\theta}_2 d_2 \cos\theta_2$$

(3)

where $\dot{x}_1$ and $\dot{y}_1$ are the linear velocities of the front module, and $\dot{\theta}_1$ and $\dot{\theta}_2$ are the rotational velocities of the first and second modules, respectively. Differentiating Equation (2) again yields the linear accelerations, $(\ddot{x}_2, \ddot{y}_2)$, of the second module:

$$\ddot{x}_2 = \ddot{x}_1 - \ddot{\theta}_1 d_1 \sin\theta_1 - \dot{\theta}_1^2 d_1 \cos\theta_1 - \ddot{\theta}_2 d_2 \sin\theta_2 - \dot{\theta}_2^2 d_2 \cos\theta_2$$
$$\ddot{y}_2 = \ddot{y}_1 + \ddot{\theta}_1 d_1 \cos\theta_1 - \dot{\theta}_1^2 d_1 \sin\theta_1 + \ddot{\theta}_2 d_2 \cos\theta_2 - \dot{\theta}_2^2 d_2 \sin\theta_2$$

(4)

where $\ddot{x}_1$ and $\ddot{y}_1$ are the linear accelerations of the front module, and $\ddot{\theta}_1$ and $\ddot{\theta}_2$ are the rotational accelerations of the first and second modules, respectively.

The inertial linear velocities of a drive module are related to its forward velocity v_{xi} in a body-centric frame:

$$\dot{x}_i = v_{xi} \cos\theta_i$$
$$\dot{y}_i = v_{xi} \sin\theta_i$$

(5)

where $i = 1,2$, and 1 refers to the front module while 2 refers to the rear module. The body-centric forward velocity of module i is related to its left and right wheel rotational velocities:

$$v_{xi} = \frac{r_w\left(\omega_{ri} + \omega_{li}\right)}{2}$$

(6)

where r_w is the wheel radius, ω_{ri} is the right wheel rotational velocity and ω_{li} is the left wheel rotational velocity. The rotational velocity of a drive module is also related to its wheel velocities:

$$\dot{\theta}_i = \frac{r_w\left(\omega_{ri} - \omega_{li}\right)}{w}$$

(7)

where w is the distance between the right and left wheels of the drive module.

If the front and rear modules are to follow the same circular path on the plane, there will be a yaw joint angle $\theta_{j,d}$ that will permit the rear module to follow the front module. Consider the moment the front module enters a curve, while the rear module maintains its previous heading. The instantaneous center of rotation of the front module, r_{IC}, is:

$$r_{IC} = \frac{w\left(\omega_{r1} + \omega_{l1}\right)}{2\left(\omega_{r1} - \omega_{l1}\right)} \tag{8}$$

The path length s that must be traveled by the rear module before it enters the same curve is

$$s = r_{IC}\theta_d = d_1 + d_2 \tag{9}$$

At the moment the rear module enters the curve, the angle θ_d is the difference in orientation between the front and rear modules. This angle can be calculated from the instantaneous center of rotation by rewriting Equation (9):

$$\theta_d = \frac{d_1 + d_2}{r_{IC}} = \frac{2\left(d_1 + d_2\right)\left(\omega_{r1} - \omega_{l1}\right)}{w\left(\omega_{r1} + \omega_{l1}\right)} \tag{10}$$

Note that if the robot is traveling on a straight path, r_{IC} is infinite and the desired joint angle is 0.

3. LEADER-FOLLOWER FEEDBACK CONTROLLER

A simple leader-follower controller is desired so that the rear module follows the same path as the front module. The user directly drives the front module using a joystick, which sends forward and turning velocity commands that are converted into left and right motor speeds. The leader-follower controller must determine the commands to send to the right and left rear motors. For straight-line motion, one could simply match all the motor speeds, but this will not work while turning. As described in Section 2, there is a path-dependent yaw joint angle that permits the rear module to follow the front module regardless of the path curvature. Using the kinematic equations above, a feedback controller that drives the yaw joint angle to the desired angle can be implemented.

Figure 5 shows the control block diagram for the proposed leader-follower controller. The user sends linear and angular velocity commands to the front module which are translated into left and right motor speed commands. These motor speed commands are used to calculate the desired yaw joint angle using Equation (10). Sensor feedback is used to calculate the error between the desired and measured joint angle. PID control on this error and an additional kinematic constraint are applied to determine the right and left rear motor speed commands, as explained below. Note that each motor also has its own individual controller.
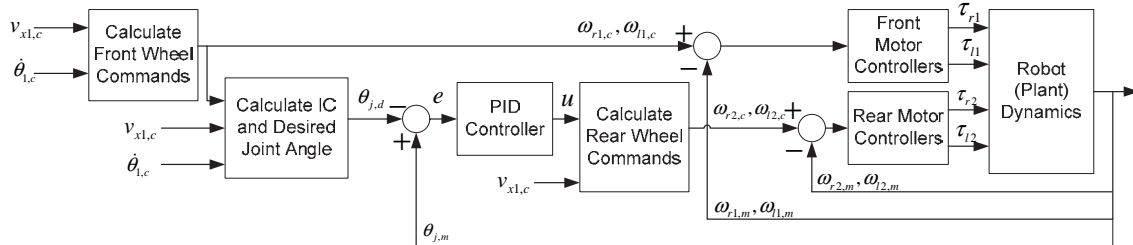

Figure 5. Leader-follower control block diagram.

The robot is equipped with wheel encoders, an IMU on each module, and an angular position sensor on its yaw joint. The error between the desired and measured joint angle is calculated as:

$$e = \theta_{j,m} - \theta_d \tag{11}$$

where $\theta_{j,m}$ is the measured joint angle. The change in this error can be calculated using the encoder measurements from both sets of wheels:

$$\dot{e} = \dot{\theta}_1 - \dot{\theta}_2 = \frac{r_w\left(\omega_{r,1} - \omega_{l,1} - \omega_{r,2} + \omega_{l,2}\right)}{w} \tag{12}$$

Using these errors, a PID control law can be defined:

$$u = K_p e + K_I \int e\,dt + K_D \dot{e} \tag{13}$$

where u is the commanded angular velocity of the rear module, and K_p, K_I and K_D are the proportional, integral and derivative gains, respectively. The angular position error in Equation (13) can be numerically integrated with sufficient anti-windup included in the software implementation.

Both a forward velocity and angular velocity are needed to determine the right and left wheel commands. The angular velocity command is determined by the PID controller. The robot geometry constrains the forward speed of the second module, since there is no compliance in the yaw linkage. Hence, the magnitudes of the forward velocities of both modules must remain the same so they stay connected. Therefore:

$$v_{x,2c} = v_{x,1c} \tag{14}$$

The left and right rear motor speed commands, $\omega_{2,r,c}$ and $\omega_{2,l,c}$, can be determined by:

$$\begin{bmatrix} \omega_{2,r,c} \\ \omega_{2,l,c} \end{bmatrix} = \begin{bmatrix} \dfrac{1}{r_w} & \dfrac{w}{2r_w} \\ \dfrac{1}{r_w} & \dfrac{-w}{2r_w} \end{bmatrix} \begin{bmatrix} v_{x,2c} \\ u \end{bmatrix} \tag{15}$$

The robot geometry imposes limits on its permissible trajectories. The yaw joint has a range of (-45/45) degrees, which restricts the robot's ability to maneuver in a tight circle. Hence, there is a minimum instantaneous center of rotation that limits the difference between the right and left motor speeds. This constraint is found by substituting the maximum range into Equation (10) and rearranging:

$$\left|\omega_r - \omega_l\right| < \frac{\pi w\left(\omega_{r1} + \omega_{l1}\right)}{8\left(d_1 + d_2\right)} \tag{16}$$

A model of the MSMR dynamics is needed to emulate its behavior when testing the leader-follower PID controller in simulation. Assume that the magnetic force between the wheels and the planar surface the robot travels on acts orthogonally to the robot motion. The following state model can be derived from first principles:

$$\mathbf{M(q)}\dot{\mathbf{v}} + \mathbf{H(v,q)} + \mathbf{P(q)v} = \mathbf{Bu} \tag{17}$$

where $\mathbf{v}$ is the state vector, $\mathbf{M(q)}$ is the mass matrix, vector $\mathbf{H(v,q)}$ contains centripetal terms, $\mathbf{P(q)}$ is the dissipative matrix, $\mathbf{B}$ is the input matrix and $\mathbf{u}$ is the control vector. The individual terms of the matrices are found in the Appendix. The state vector $\mathbf{v}$ is defined as

$$\mathbf{v} = \begin{bmatrix} \omega_{r1} & \omega_{l1} & \omega_{r2} & \omega_{l2} & i_{r1} & i_{l1} & i_{r2} & i_{l2} \end{bmatrix}^T \tag{18}$$

where i is motor current. The system inputs are the voltages applied to the motors:

$$\mathbf{u} = \begin{bmatrix} V_{r1} & V_{l1} & V_{r2} & V_{l2} \end{bmatrix}^T \tag{19}$$

The PID controller was tuned and partially tested in Matlab Simulink before implementation on the MSMR. Physical parameters used in the simulation are listed in Table 1.

Table 1. Physical parameters for simulation.

Module mass m	2.5 kg
Distance d_1	0.1303 m
Distance d_2	0.1278 m
Width w	0.2692 m
Wheel radius r_w	0.0508 m
Front module inertia I_1	0.0252 kg-m^2
Rear module inertia I_2	0.0249 kg-m^2
Gear box ratio N	128
Motor torque constant K_T	0.0208 N-m/A
Motor voltage constant K_V	0.0208 V/rad/s
Motor inductance L	0.186 mH
Motor resistance R	1.53 Ohms
Motor inertia J	1.47x10^{-5} kg-m^2
Motor rotational friction b	0.01 N-m/rad/s

In simulation, the robot was commanded to follow circular paths at various forward speeds, and the controller gains were tuned iteratively. Figure 6 and Figure 7 show the simulated position histories of the front and rear modules at forward velocities of 8 cm/s and 20 cm/s, respectively. Note that the robot has a maximum forward speed of approximately 30 cm/s, but is unable to turn while maintaining that forward speed. In both instances, the rear module path converges to the front module path, albeit more quickly at lower forward speed. The controller gains that resulted in satisfactory performance under a wide variety of trajectories, including the two presented are proportional gain K_P of 1, integral gain K_I of 2 and derivative gain K_D of 0.5. These gains are used as starting points for physical implementation.
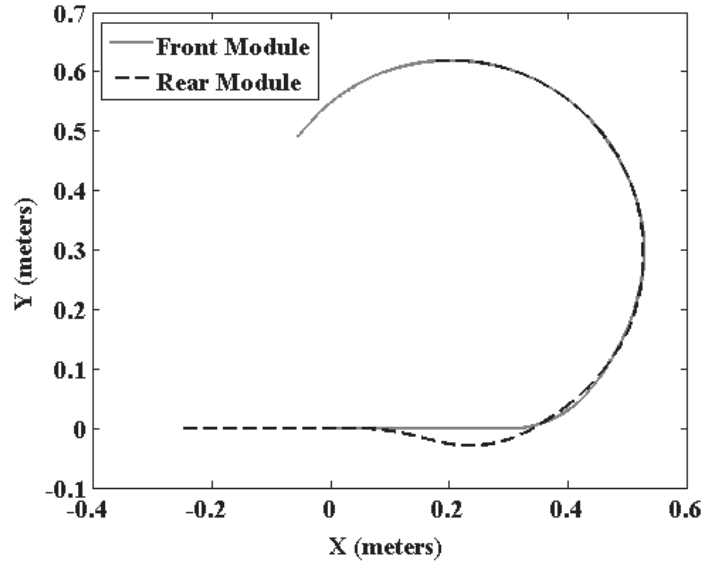
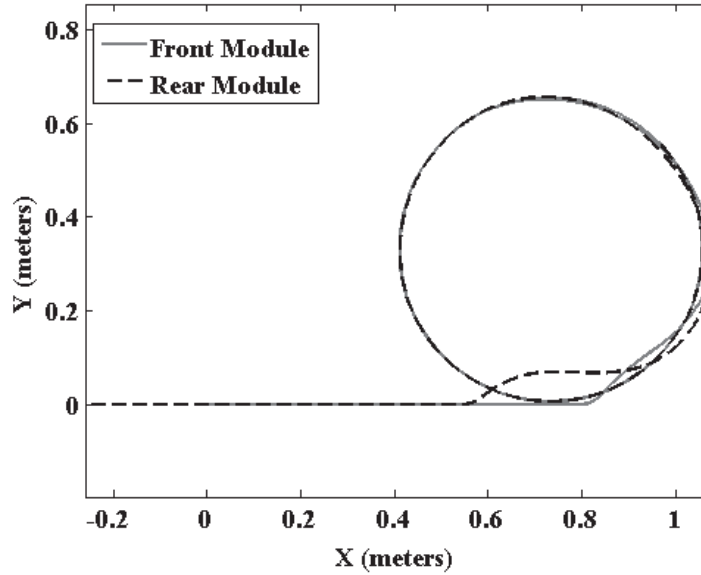Figure 6. Front and rear module position history, mean velocity 8 cm/s.

Figure 7. Front and rear module position history, mean velocity 20 cm/s.

4.   EXPERIMENTAL RESULTS

To test the validity of MSMR with a leader-follower controller, a number of experiments were run on a large flat metal surface as shown in Figure 8 and Figure 9. A cylinder with a dry erase marker was taped to each robot module so that a line would be scribed on the ground to illustrate the path of each module. A blue marker was used for the leading module and red for the trailing module.

The first experiment consisted of testing MSMR at a velocity of 8 cm/s using the PID values found in simulation (Figure 6). The simulation results exhibited a deviation (illustrated by the dashed line as it transitions from the straight line to

the circle in Figure 6) than the experimental result. The absence of overshoot in the real-world experiment was likely due to the ability of the robot to overpower the bond between the wheel magnets and the metal surface, causing wheel slip that was not allowed during the simulation. However, during the experiment the robot exhibited an undesired oscillatory trajectory while following the prescribed path (see Figure 8). This behavior was likely created by a combination of aggressive PID values (specifically the high derivative gain) and small differences between the simulated and experimental physical parameters.
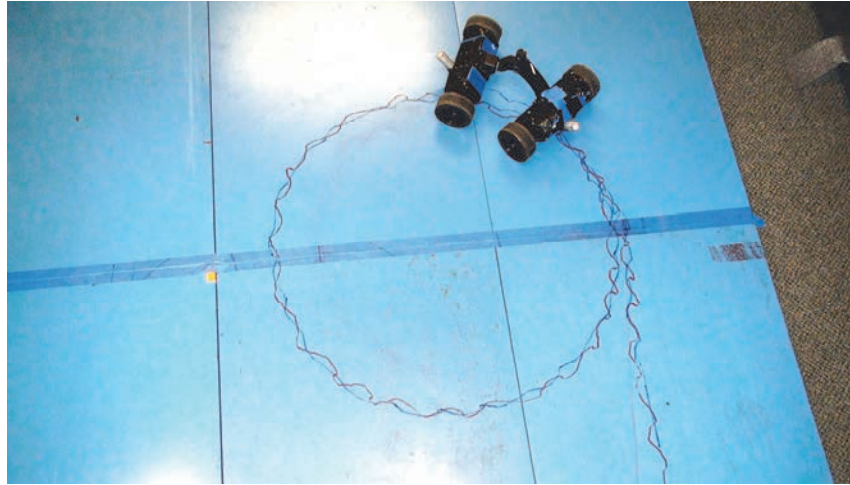

Figure 8. MSMR Driving a Loop with PID Gains K_P=1, K_I=2, K_D=0.5, mean velocity 8 cm/s. The blue trace was drawn by a marker attached to the front module, and the red trace was drawn by one attached to the rear module.

In the next set of experiments, the MSMR was driven in a path at varied speeds along circles of different diameters. During the course of these experiments, the physical limitations of the MSMR were measured (i.e. actuator saturation, maximum angular rate, minimum turn radius) and compared to what had been coded in the simulations. Throughout these experiments the PID controller was iteratively tuned until acceptable gains were found. A PI controller with gains, K_P = 0.35, K_I=5.0e-5, and K_D=0 was found to be sufficient to allow for good path convergence of the rear module to the front module.

With the new controller gains, the first experiment was run again. MSMR did significantly better at following the circular path with both modules in this case (see Figure 9). The trajectory shows the rear module (red line) tracking the front module (blue line) with very little error and both modules closing the circular path they were driving.

Figure 9. MSMR Driving a Loop with PI Gains K_P=0.35, K_I=5.0e-5, mean velocity 8 cm/s.

5. CONCLUSIONS

A simple leader-follower controller for the MSMR robot is developed. A kinematic analysis of its motion shows that for every instantaneous center of rotation of the front module, there is a corresponding yaw joint angle that permits the rear module to follow the front module. Leader-follower control is achieved by applying PID control on the error between the measured and desired yaw joint angle to determine the rear motor speeds. The controller concept is tested in simulation, and then implemented in hardware. Experiments show that, with appropriate tuning, the simple leader-follower controller developed and presented in this paper is sufficient in controlling the MSMR.

ACKNOWLEDGEMENT

REFERENCES

[1] Tâche, F., Fischer, W., Siegwart, R., Moser, R. and Mondada, F., "Compact magnetic wheeled robot with high mobility for inspecting complex shaped pipe structures," IEEE/RSJ Int. Conf. on Intelligent Robots and Systems (IROS) 2007, 261-266 (2007).

[2] Tâche, F., Fischer, W., Caprari, G., Siegwart, R., Moser, R. and Mondada, F., "Magnebike: A magnetic wheeled robot with high mobility for inspecting complex-shaped structures," Journal of Field Robotics, 26, 453-476 (2009).

[3] Eich, M. and Vogele, T., "Design and control of a lightweight magnetic climbing robot for vessel inspection," 19th Mediterranean Conf. on Control & Automation (MED), 1200-1205 (2011).

[4] Eiammanussakul, T., Taoprayoon, J. and Sangveraphunsiri, V., "Weld Bead Tracking Control of a Magnetic Wheel Wall Climbing Robot Using a Laser-Vision System," Applied Mechanics and Materials, 219-223 (2014).

[5] Yi, Z., Gong, Y., Wang, Z. and Wang, X., "Development of a wall climbing robot for ship rust removal," Int. Conf. on Mechatronics and Automation (ICMA), 4610-4615 (2009).

[6] Leon-Rodriguez, H., Hussain, S. and Sattar, T., "A compact wall-climbing and surface adaptation robot for non-destructive testing," 12th Int. Conf. on Control, Automation and Systems (ICCAS), 404-409 (2012).

[7] Fernández, R., González, E., Feliú, V. and Rodríguez, A. G., "A wall climbing robot for tank inspection. An autonomous prototype," in 36th Annual Conf. on IEEE Industrial Electronics Society, 1424-1429 (2010).

[8] Kitai, S., Tsuru, K. and Hirose, S., "The proposal of swarm type wall climbing robot system 'Anchor Climber'— the design and examination of adhering mobile unit," IEEE/RSJ Int. Conf. on Intelligent Robots and Systems (IROS), 475-480 (2005).

[9] Silva, M. F., Barbosa, R. S. and Oliveira, A. L. C., "Climbing Robot for Ferromagnetic Surfaces with Dynamic Adjustment of the Adhesion System," Journal of Robotics, 2012, (2012).

[10] Lee, G., Seo, K., Lee, S., Park, J., Kim, H., Kim, J. and Seo, T., "Compliant track-wheeled climbing robot with transitioning ability and high-payload capacity," 2011 IEEE Int. Conf. on Robotics and Biomimetics (ROBIO), 2020-2024 (2011).

[11] Espinoza, R. V., de Oliveira, A. S., de Arruda, L. V. R. and Neves Junior, F., "Navigation's Stabilization System of a Magnetic Adherence-Based Climbing Robot," Journal of Intelligent & Robotic Systems, 1-17 (2014).

[12] Lee, G., Wu, G., Kim, S. H., Kim, J. and Seo, T., "Combot: Compliant climbing robotic platform with transitioning capability and payload capacity," 2012 IEEE Int. Conf. on Robotics and Automation (ICRA), 2737-2742 (2012).

[13] Wang, H., Huang, X., Hong, R. and Fang, C., "A new inspection robot system for storage tank," 7th World Congress on Intelligent Control and Automation (WCICA), 7427-7431 (2008).

[14] Lee, W., "Proposition of reconfigurable wall climbing robot using 6DOF force torque sensor based on flexible structure for real environment," 13th Int. Conf. on Control, Automation and Systems (ICCAS), 1802-1806 (2013).

[15] Erdmann, C. R., "080727-N-4236E-155," United States Navy, <http://www.navy.mil/view_image.asp?id=62050> (2008).

[16] Burmeister, A., Pezeshkian, N., Talke, K., Ostovari, S., Everett, H.R., Hart, A., Gilbreath, G. and Nguyen, H.G., "Design of a Multi-Segmented Magnetic Robot for Hull Inspection," Naval Engineers Journal, 126-3, 53-60 (2014).

[17] Kamegawa, T., Yarnasaki, T., Igarashi, H. and Matsuno, F., "Development of the snake-like rescue robot 'kohga'," IEEE Int. Conf. on Robotics and Automation (ICRA '04), 5081-5086 (2004).

[18] Laumond, J. P., Sekhavat, S. and Lamiraux, F., "Guidelines in nonholonomic motion planning for mobile robots," Robot Motion Planning and Control, 229, 1-53 (1998).

[19] Tanaka, M. and Matsuno, F., "Experimental Study of Redundant Snake Robot Based on Kinematic Model," 2007 IEEE Int. Conf. on Robotics and Automation, 2990-2995 (2007).

[20] Agrawal, S. K. and Chang, S., "Trajectory of a Multi-segment Wheeled Vehicle," Mechanics of Structures and Machines, 24, 389-404 (1996).

[21] Matsuno, F. and Suenaga, K., "Control of redundant snake robot based on kinematic model," Proc. 41st SICE Annual Conference, 3, 1481-1486 (2002).

[22] Tilbury, D., Laumond, J. P., Murray, R., Sastry, S. and Walsh, G., "Steering car-like systems with trailers using sinusoids," 1992 IEEE Int. Conf. on Robotics and Automation, 3, 1993-1998 (1992).

[23] Laumond, J. P., "Controllability of a multibody mobile robot," IEEE Transactions on Robotics and Automation, 9, 755-763 (1993).

[24] Lamiraux, F., Sekhavat, S. and Laumond, J. P., "Motion planning and control for Hilare pulling a trailer," IEEE Transactions on Robotics and Automation, 15, 640-652 (1999).

[25] Lee, J.-H., Chung, W., Kim, M. and Song, J.-B., "A passive multiple trailer system with off-axle hitching," Int. Journal of Control Automation and Systems, 2, 289-297 (2004).

[26] Nakamura, Y., Ezaki, H., Tan, Y. and Chung, W., "Design of steering mechanism and control of nonholonomic trailer systems," IEEE Transactions on Robotics and Automation, 17, 367-374 (2001).

[27] Sampei, M., Tamura, T., Itoh, T. and Nakamichi, M., "Path tracking control of trailer-like mobile robot," Proc. IEEE/RSJ Int. Workshop on Intelligent Robots and Systems: Intelligence for Mechanical Systems (IROS '91), 1, 193-198 (1991).

[28] Yuan, J., Huang, Y., Kang, Y. and Liu, Z., "A Strategy of Path Following Control for Multi-Steering Tractor-Trailer Mobile Robot," IEEE Int. Conf. on Robotics and Biomimetics (ROBIO 2004), 163-168 (2004).

[29] Michałek, M. M., "A highly scalable path-following controller for N-trailers with off-axle hitching," Control Engineering Practice, 29, 61-73 (2014).

APPENDIX

Dynamic Model Matrices

The terms in the mass matrix $\mathbf{M}(\mathbf{q})$ are:

$$M_{1,1} = \frac{NJ}{r_w}\cos\theta_1 + \frac{r_w(m_1+m_2)}{2}\cos\theta_1 + \frac{2r_w m_2(d_1\sin\theta_1)}{w}$$

$$M_{1,2} = \frac{NJ}{r_w}\cos\theta_1 + \frac{r_w(m_1+m_2)}{2}\cos\theta_1 - \frac{2r_w m_2(d_1\sin\theta_1)}{w}$$

$$M_{1,3} = \frac{NJ}{r_w}\cos\theta_2 + \frac{2r_w m_2(d_2\sin\theta_2)}{w}$$

$$M_{1,4} = \frac{NJ}{r_w}\cos\theta_2 - \frac{2r_w m_2(d_2\sin\theta_2)}{w}$$

$$M_{2,1} = \frac{NJ}{r_w}\sin\theta_1 - \frac{2r_w m_2(d_1\cos\theta_1)}{w}$$

$$M_{2,2} = \frac{NJ}{r_w}\sin\theta_1 + \frac{2r_w m_2(d_1\cos\theta_1)}{w}$$

$$M_{2,3} = \frac{NJ}{r_w}\sin\theta_2 - \frac{2r_w m_2(d_2\cos\theta_2)}{w}$$

$$M_{2,4} = \frac{NJ}{r_w}\sin\theta_2 + \frac{2r_w m_2(d_2\cos\theta_2)}{w}$$

$$M_{3,1} = \frac{2r_w I_1}{w} + \frac{NJw}{2r_w}$$

$$M_{3,2} = -\frac{2r_w I_1}{w} - \frac{NJw}{2r_w}$$

$$M_{3,3} = \frac{NJwd_1 \sin(\theta_1 - \theta_2)}{2r_w}$$

$$M_{4,3} = \frac{2r_w I_2}{w} + \frac{NJw}{2r_w}$$

$$M_{3,4} = \frac{NJwd_1 \sin(\theta_1 - \theta_2)}{2r_w}$$

$$M_{4,4} = -\frac{2r_w I_2}{w} - \frac{NJw}{2r_w}$$

$$M_{4,1} = -\frac{NJwd_2 \sin(\theta_1 - \theta_2)}{2r_w}$$

$$M_{5,5} = M_{6,6} = M_{7,7} = M_{8,8} = L$$

$$M_{4,2} = -\frac{NJwd_2 \sin(\theta_1 - \theta_2)}{2r_w}$$

where m_i is the mass of the ith module, N is the gearbox ratio between the motor and the wheel, J is the rotational inertia of the motor, I_i is the inertia of the ith module, and L is the motor inductance.

The vector $\mathbf{H}(\mathbf{v}, \mathbf{q})$ is:

$$\mathbf{H}(\mathbf{v}, \mathbf{q}) = \begin{bmatrix} m_2 d_1 \cos\theta_1 \left(\frac{2r_w}{w}\right)^2 (\omega_{r1} - \omega_{l1})^2 + m_2 d_2 \cos\theta_2 \left(\frac{2r_w}{w}\right)^2 (\omega_{r2} - \omega_{l2})^2 \\ m_2 d_1 \sin\theta_1 \left(\frac{2r_w}{w}\right)^2 (\omega_{r1} - \omega_{l1})^2 + m_2 d_2 \sin\theta_2 \left(\frac{2r_w}{w}\right)^2 (\omega_{r2} - \omega_{l2})^2 \\ 0 \\ 0 \\ 0 \\ 0 \\ 0 \\ 0 \end{bmatrix}$$

The terms in the dissipative matrix $\mathbf{P}(\mathbf{q})$ are:

$$P_{1,1} = P_{1,2} = Nb \cos\theta_1$$
$$P_{1,3} = P_{1,4} = Nb \cos\theta_2$$
$$P_{1,5} = P_{1,6} = -NK_m \cos\theta_1$$
$$P_{1,7} = P_{1,8} = -NK_m \cos\theta_2$$
$$P_{2,1} = P_{2,2} = Nb \sin\theta_1$$
$$P_{2,3} = P_{2,4} = Nb \sin\theta_2$$
$$P_{2,5} = P_{2,6} = -NK_m \sin\theta_1$$
$$P_{2,7} = P_{2,8} = -NK_m \sin\theta_2$$
$$P_{3,1} = P_{4,3} = -\frac{bNw}{2r_w}$$

$$P_{3,2} = P_{4,4} = \frac{bNw}{2r_w}$$

$$P_{3,3} = P_{3,4} = d_1 \frac{bN}{r_w} \sin(\theta_1 - \theta_2)$$

$$P_{3,5} = P_{4,7} = -\frac{K_m Nw}{2r_w}$$

$$P_{3,6} = P_{4,8} = \frac{K_m Nw}{2r_w}$$

$$P_{3,7} = P_{3,8} = -d_1 \frac{K_m N}{r_w} \sin(\theta_1 - \theta_2)$$

$$P_{4,1} = P_{4,2} = -d_2 \frac{bN}{r_w} \sin(\theta_1 - \theta_2)$$

$$P_{4,5} = P_{4,6} = d_2 \frac{K_m N}{r_w} \sin(\theta_1 - \theta_2)$$

$$P_{5,1} = P_{6,2} = P_{7,3} = P_{8,4} = K_m$$

$$P_{5,5} = P_{6,6} = P_{7,7} = P_{8,8} = R$$

where b is the motor rotational friction constant, K_m is the motor torque constant and R is the motor electrical resistance.

The input matrix $\mathbf{B}$ is:

$$\mathbf{B} = \begin{bmatrix} 0 & 0 & 0 & 0 \\ 0 & 0 & 0 & 0 \\ 0 & 0 & 0 & 0 \\ 0 & 0 & 0 & 0 \\ 1 & 0 & 0 & 0 \\ 0 & 1 & 0 & 0 \\ 0 & 0 & 1 & 0 \\ 0 & 0 & 0 & 1 \end{bmatrix}$$